Extended Abstracts of the 2008 International Conference on Solid State Devices and Materials, Tsukuba, 2008, pp. 118-119

F-1-1 (Invited)

Semiconductor Nanowires: from Growth to Device Applications

D. L. Kwong[1*], G. Q. Lo[1], J. D. Ye[1], S. T. Tam[1], S. J. Lee[2], and X. W. Sun[3]

[1]Institute of Microelectronics, A*STAR, 11 Science Park Road, Singapore, 117685; [2]SNDL, ECE, National University of Singapore, Singapore, 117576; [3]EEE, Nanyang Technological University, Singapore, 639654. [*]kwongdl@ime.a-star.edu.sg

Introduction

This talk provides an overview of recent semiconductor nanostructure research efforts from research organizations in Singapore in aspects of wire-based material synthesis towards applications oriented device development.

Specifically, synthesis covers from CVD growth of Si-, SiGe nanowires along with the doping impacts, to various ZnO-nanostructures from hydrothermal technique in comparison with MOCVD growth. From device analysis, carrier transport and Schottky barrier are analyzed for Si-, SiGe nanowires. More so for ZnO nanostructures, many applications and devices will be discussed, e.g., for field emission using diode and triode configurations, ZnO/Si heterojunction LED and ZnO nanowire/$CuAlO_2$ heterojunction LED, in gas and biochemical sensing, in dye-sensitized solar cells, and lastly on electrochromic display (electronic paper) making use of ZnO nanorod electrode.

CVD Si-, SiGe-NW based on Bottom-up Approach

Si/Ge nanowires were synthesized by using either mono-dispersed 10-20 nm Au colloids or a 10 nm evaporated Al-seeds on SiO_2-substrate. Si nanowires were grown at 440 °C in SiH_4 for Au- or at 540 °C for Al-catalyst. SiH_4 and GeH_4 were simultaneously introduced in reactor to grow $Si_{1-x}Ge_x$. [B]-doping was done either by B_2H_6 during growth or by *in situ* RF plasma after growth. The harvested wires were suspended in ethanol solution by ultra sonication and deposited onto substrates.

Forming back gated MOSFETs, a TaN/Ta electrode was sputtered, followed by ALD (300 °C, $HfCl_4$) HfO_2 ~5 nm, on which crystalline phosphorus doped Si or SiGe wires were dispersed. Lift-off was used to form Pd-S/D electrodes.

Fig. 1 shows the Si NWs (~20 nm) on Al seeding. AES confirms the Al existence at the tip of wire, whereas no Al in mid-section. The crystalline core and ultra-thin surrounding α-layer are confirmed by TEM. Adding B_2H_6 in Au-catalyzed growth, significantly different growth morphology was observed [**Fig. 2**], with marked reduction in density and length of NWs, and a cone-shaped structure. However, such was not observed in case of Al-catalyzed. Such difference can be explained by the phase diagrams of Au–B and Al–Si systems. Alternatively, post-synthesis *in situ* plasma B_2H_6 doping after Si NW growth without dopant gas was also studied. Analysis [**Fig. 3**] shows that good morphology and crystallinity of undoped nanowires can be maintained.

For SiGe, processes at 430 vs. at 450 °C showed differences in microstructure and morphology. 430C resulted in single crystalline homogeneous SiGe NW, whereas T>450C resulted in thick α-outer layer. Post-synthesis *in situ* plasma PH_3 doping was carried out. Analysis indicates P-incorporation can be controlled by process time and 10^{19} cm^{-3} with 10nm depth, with affecting the microstructure and morphology.

This talk will discuss the device characteristics from devices made from these wires. Examples are shown **Fig. 4** -- p-MOSFET operations are observed without showing the ambipolar behavior. This could be due to the suppressed electron transport with high barrier heights at the S/D edges.

ZnO-Nano-Structure Synthesis and Applications

Due to its wide direct bandgap (3.37eV) with a large exciton binding energy (60 meV), ZnO is considered as a promising candidate for blue, UV, and white LEDs. In addition to the effort of achieving reliable p-ZnO, the wish for ZnO/Si heterostuctured LEDs has stirred-up considerable interest. However, epitaxial growth of ZnO on Si is difficult due to the large lattice mismatch and Si-surface oxidation.

Besides potentially being the brightest inorganic emitting material, ZnO has other wide application areas, e.g., transparent conductor, varistor, surface acoustic wave device, gas sensor, photo-catalysis, thin film transistor. Interestingly, with the increasing interests in low-dimensional materials, ZnO has been proven to exhibit the richest nanostructures of all. Being in the nano form, besides quantum confinement effect (not much experiment on this yet as the size is generally larger than 10 nm), surface area also increases tremendously, which makes it effective for applications such as gas sensing and large dye-loading in dye-sensitized solar cells.

For nano-structure synthesis, ZnO (primarily nanowires, rods) can be formed by a very low temperature process (<90°C) by the aqueous thermal decomposition method (also called hydrothermal method) [**Fig. 5**].

In addition to the discussion of ZnO synthesis, we will also review the device works. Examples include (1) iso-type epi-n-ZnO/n-Si(111) heterojunction light-emitting diode with a MgO/TiN buffer, which is fully integrate-table to CMOS; (2) a nanostructure ZnO gas sensor based on tubular ZnO and its response to CO [**Fig. 5**]; and (3) a highly bendable ZnO nanowire electrode and its application as photoanode in dye-sensitized solar cells [**Fig. 6**].

Summary

In this talk, several nano-structure semiconductor materials and synthesis are discussed, specifically on Si-/Ge-nanowires, and ZnO-low-dimensional structures. The device and applications will be analyzed in depth.

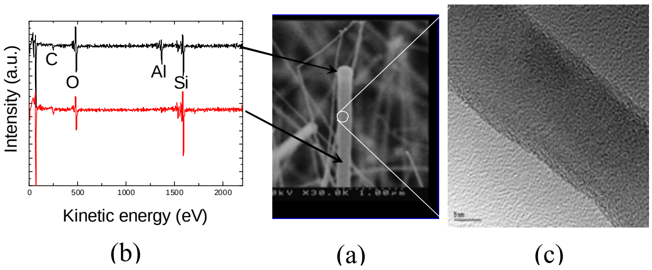

Fig. 1 (a) SEM image of Si NWs synthesized with Al catalyst, showing the existence of spherical Al catalyst at the tip of the nanowire after VLS growth, (b) AES results on the tip of the NW and on the middle of the NW. Al is detected at the tip of the nanowire, (c) TEM image of Si NWs with a diameter of ~20 nm.

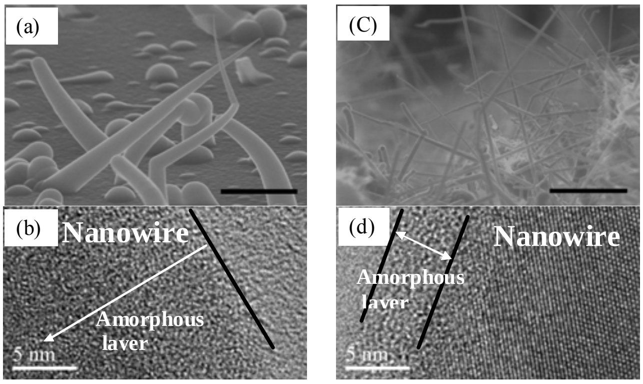

Fig. 2. (a) SEM image of Au-catalyzed Si NW with co-flowing SiH_4 and B_2H_6 gases (scale bar 3 μm). (b) TEM image of the edge of the Au-catalyzed Si NW with co-flowing SiH_4 and B_2H_6 gases: a thick amorphous layer is observed without a crystalline lattice. (c) SEM image of Al-catalyzed Si NW with co-flowing SiH_4 and B_2H_6 gases (scale bar 3 μm). (d) TEM image of the edge of the Al-catalyzed Si NW with co-flowing SiH_4 and B_2H_6 gases: a crystalline lattice is clearly observed with a thin amorphous layer.

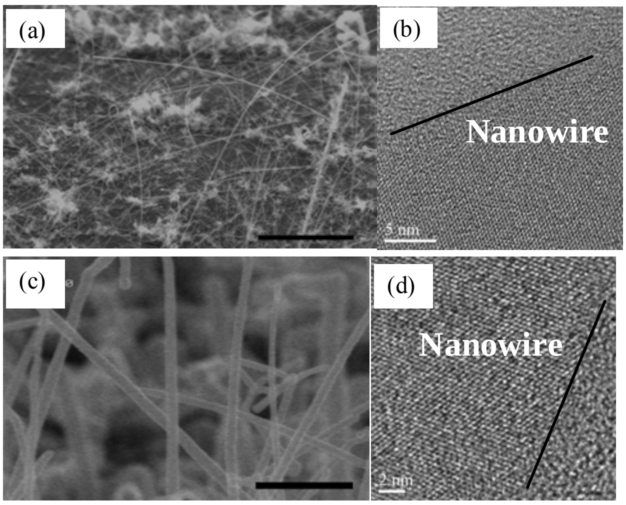

Fig. 3. (a) SEM image of Au-catalyzed Si NW with post-synthesis plasma B_2H_6 doping (scale bar 3 μm). (b) TEM image of the the edge of the Au-catalyzed Si NW with post-synthesis plasma B_2H_6 doping. (c) SEM image of Al-catalyzed Si NW with post-synthesis plasma B_2H_6 doping (scale bar 3 μm). (d) TEM image of the edge of the Al-catalyzed Si NW with post-synthesis plasma B_2H_6 doping.

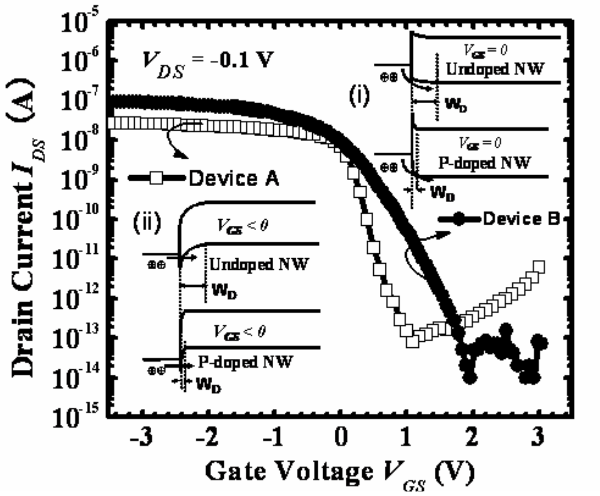

Fig. 4. Typical I_{DS}–V_{GS} transfer characteristics (Inset (i) shows a comparison of depletion width (W_D) in the band diagram of the metal/Si1−xGex NW at source region under thermal equilibrium status. Inset (ii) shows a comparison of W_D in the band bending diagram of the metal/SiGe NW interface at source region under negative gate bias condition.

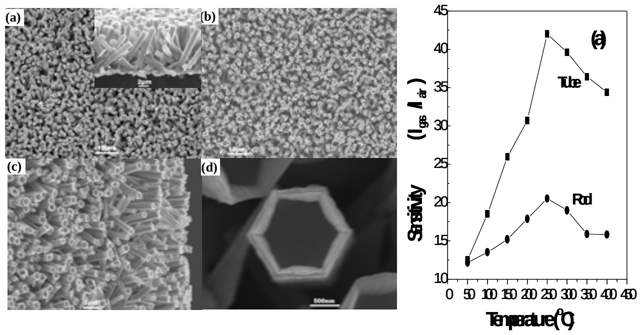

Fig. 5 SEM images of the ZnO rods synthesized by aqueous thermal decompositions, with (a) to (d) representing different zoom-in scale. The sensitivities of the ZnO tube and rods are compared as a function of temperatures as the structures exposed to CO testing gas (250ppm).

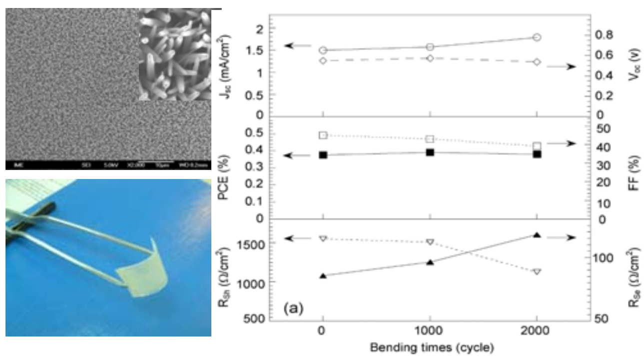

Fig. 6. (Left) SEM images of the electrode and a bended electrode. (Right) Graphs the photovoltaic characteristics for devices being bent under stress and numbers of cycles of bending for a dye-sensitized solar-cell devices with ZnO nanostructures as the electrode.